Nano Energy 65 (2019) 104059

Contents lists available at ScienceDirect

Nano Energy

journal homepage: www.elsevier.com/locate/nanoen

Full paper

Self-pumped evaporation for ultra-fast water desalination and power generation

Ji Li, Shan Gao, Rui Long, Wei Liu**, Zhichun Liu*

School of Energy and Power Engineering, Huazhong University of Science and Technology, Wuhan, 430074, China

ARTICLE INFO

Keywords:
Desalination
New energy
Low-grade heat
Water pump
Molecular dynamics

ABSTRACT

Getting fresh water and electricity by utilizing low-grade thermal energy are attractive to deal with the global resource crisis. Here, a self-pumped evaporation regime based on charged carbon nanotubes membrane is reported, which can purify water and output power efficiently with thermal energy supplied. Using molecular dynamics simulations, ultra-high desalination rates of 3.6 ± 0.5 g/(cm^{2}s) and power generation rates of 170 ± 24 W/cm^2 were gotten with temperature difference of 40 K. The causes of the super rates include high pump capacity, low thermal resistance, and low irreversibility. This study shows a promising approach to desalinate water and generate power efficiently by consuming low-grade heat.

1. Introduction

As global water and energy issues are becoming more and more urgent, it is attractive to desalt water and get power by utilizing the huge amounts of thermal energy from solar, geothermy, metallurgy, thermal power generation, and other activities [1]. However, this work is very challenging because thermal energy is low-grade and difficult to converse especially for low temperature sources.

Desalination needs to consume external energy to overcome the chemical potential difference, $\Delta\mu$ between saline and pure water. The $\Delta\mu$ induces the osmosis pressure difference, Δp_o in liquids and saturation pressure difference, Δp_s in vapors. And water trends to move from freshwater to solution by driving forces of Δp_o or Δp_s. Reverse osmosis (RO) and thermal distillation are the two main desalination methods applied in business. RO applies saline water external pressures to overcome Δp_o to drive water moving across membrane from salt to fresh side. With membrane and pump technology developing quickly, RO gets most market share and attention for its flexibility, simplicity, and efficiency [2–5]. Distillation consumes thermal energy to overcome the Δp_s and separate ions by vaporization, which needs to recover the condensation heat to improve its efficiency. Because of large latent phase change heat and low heat transfer ability, distillation needs large work area to get high production and efficiency, which restricts its competitiveness seriously. While thermal desalination has much potential for its ability to utilize low-grade thermal energy [6], it is very essential to strengthen thermal methods [7,8].

The heat conductivity coefficient of water is orders of magnitude lower than that of the solid wall, which is the main factor restricting the vaporization rate of a thick liquid film. In fact, vaporization can be very fast when the liquid film is thin. Heat transfer ability can be used to evaluate the capacity of vaporization device. For little thermal resistance in liquid side, nano film evaporation can reach heat fluxes on the order of 10^4 W/cm^2 with low superheat [9], although the fluxes couldn't be maintained in large plane surfaces for restriction of liquid transfer rates. By external pressure driving liquid flowing across nanoporous membrane, forced flow boiling can maintain heat fluxes of 1230 W/cm^2, equivalent to water fluxes of 0.48 g/(cm^{2}s) [10]. External driving force is not necessary for sustainable vaporization as work liquid can wet heat surface spontaneously by capillarity. Capillary pressure p_{cap} in circular pore can be estimated approximately by Young-Laplace equation: $p_{cap} = 2\sigma\cdot\cos(\theta)/r$, where σ is the liquid surface tension, r is the pore radius, and θ is the solid-liquid contact angle. So capillary pressure can be very huge when the pore radius is in nanoscale, which can even generate large negative pressures under meniscus [11,12]. Because of the strong pumping ability, capillary evaporation can get heat fluxes of 500 W/cm^2 in nanoporous membranes [13,14], and get ultra fluxes of 8500 W/cm^2 in single nano-channel [15], which can guide the design of advanced distillation system.

Getting power from low-grade heat is also important, however, it is difficult for current power generation methods to meet requirements of efficiency, rate, and flexibility simultaneously. Organic Rankine cycle is a mature method which owns high efficiency in macro system, and it

* Corresponding author.
** Corresponding author.
E-mail addresses: w_liu@hust.edu.cn (W. Liu), zcliu@hust.edu.cn (Z. Liu).

https://doi.org/10.1016/j.nanoen.2019.104059
Received 27 May 2019; Received in revised form 14 August 2019; Accepted 27 August 2019
Available online 29 August 2019
2211-2855/ © 2019 Elsevier Ltd. All rights reserved.

should be strength to perform well for small power and low temperature sources [16]. Thermoelectric method is flexible and reliable, but its efficiency is low and difficult to improve [17]. Thermal electrochemical method is more efficient but it is difficult to apply for high density sources [18]. Thermal-osmotic method is very efficient and has high potential if solving the problems including pore wetting, temperature polarization, and heat conduction loss [1,19]. Utilizing capillary flow to get power may be very potential if the radius of capillary pores are a few nanometers which can generate large driving pressures [20], and the method needs much deeper studies to explore its potential for utilizing thermal efficiently.

While capillary evaporation has large potential for distillation and power generation, it can improve the overall efficiency by combining distillation and power generation for less heat recovering processes. As capillary evaporation should work in nano pores to get the best performance for large pumping pressure, carbon nanotube (CNT) has great potential for capillary evaporation due to its outstanding properties of flow, heat conduction, and mechanical strength [21–24]. However, the hydrophilicity of CNT is not well for water without modification, which is bad for capillary flow. The interaction between carbon and water can be intensified and controlled by coulomb interaction [25]. In this paper, as shown in Fig. 1, by molecular dynamics (MD) simulations and theory analysis, it was proved firstly that self-pumping evaporation in nano pores can perform marvelously for distillation and power output with super high rates and efficiencies. When the solution is heated, the water molecules can be transported into the pore by pumping forces of capillary and coulomb, then evaporate from the solution and condense in the cooling wall, with outputting power and getting freshwater. The system has high pumping capacity, low heat resistance in liquid, low mass transfer resistance, and low heat loss, which contribute to its excellent performances.

2. Simulation methods

To get large pumping pressure, and void too large flow resistance, the section size of CNT is chosen as uncapped (18, 18), which can be connected to graphene sheets seamlessly. The length of CNT is chosen as about 6.5 nm that is enough long to confine the liquid-vapor interface in channel and can improve the system stability with superheat [10,14,26,27]. To test the potential of desalinating high concentration saline, such as underground water [2], the NaCl equivalent concentration is about 1.12 mol/L, much higher than seawater. The simulations were built, performed and visualized by packages LAMMPS and VMD [28,29]. To describe vapor and carbon properties exactly [30–33], force fields were set as CHARMM, modified TIP3P, and LCBOP [34–37]. The particle-particle-particle mesh (PPPM) method was employed to treat long-range electrostatic interactions. The model was equilibrated in NPT and NVT ensembles before main simulations with Nose-Hoover method [38,39]. NVT were the ensembles of pumping tests and saturation pressure measurement to get equilibrium properties. For evaporation processes, the temperatures of heat sources were controlled by Langevin method, and the rest parts were integrated with NVE ensembles to simulate the heat transfer process [40–42]. Simulation details are in supplemental information (SI).

3. Results and discussion

3.1. Pumping ability tests

When the system works, the power output, W_{out} can be estimated by $W_{out} = p_{load}V_{evp}$, where p_{load} is the pressure output by the piston, V_{evp} is the volume of the evaporated water. So it is necessary to test the pumping ability of the system to evaluate its potential for power output. As shown in Fig. 2-a, the pumping ability with CNT charge of -5e was tested by adding p_{load} to piston (SI 4). If p_{load} is too strong, the system will not work normally due to receding of liquid-vapor interface. As shown in Fig. 2-b, the system can provide huge pumping pressures of 45–60 MPa at temperatures of 340–400 K. Because the pumping pressure is induced by capillary and Coulomb force, and liquid surface tension decreases at high temperature, the capillary force and pumping ability increase inversely with temperature, and low temperature is beneficial to get strong pumping ability.

3.2. Evaporation simulations

As shown in Fig. 3, the desalination and power output performances of the regime with CNT charge of -5e were tested with constant heating and cooling temperatures (SP 5). Based on the results of pumping pressure tests, p_{load} for power output simulations were chosen as 40 MPa. The heating rod temperatures, T_h ranged from 340 K to 400 K. The cooling wall temperatures, T_c depended on the temperature differences, ΔT, valuing 0, 20, or 40 K. Two work states, without p_{load} added or with p_{load} = 40 MPa were tested. Results show that the rates increased with T_h and ΔT, which should because of the growth in driven forces of mass transfer, Δp_s. When p_{load} = 0, the system was in self-pumped distillation state without power output, and got best distillation rates of 6.0 ± 0.5 g/(cm^{2}s) with T_h = 400 K, ΔT = 40 K. When added p_{load} of 40 MPa, the system can generate pure water and power synchronously, and got max mass fluxes of 3.6 ± 0.5 g/(cm^{2}s) and power generation rate of 170 ± 24 W/cm^2 with T_h = 400 K, ΔT = 40 K. Furthermore, it is observed that the mass fluxes were negative when ΔT = 0 K, and the mass fluxes got reduced with p_{load} added at same temperature conditions.

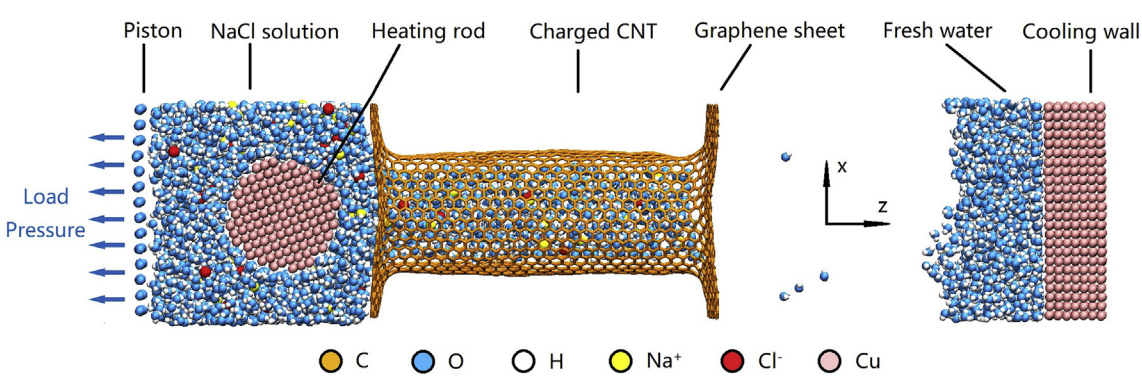

Fig. 1. Figure of the simulation model, and it contains a piston, a NaCl solution, a copper heater, two graphene sheets, a charged CNT, a freshwater film, and a copper condensation wall. The NaCl equivalent concentration is about 1.12 mol/L, much higher than the seawater. Load pressure can be added to piston atoms uniformly, and the evaporation of water molecules can overcome it to output power.

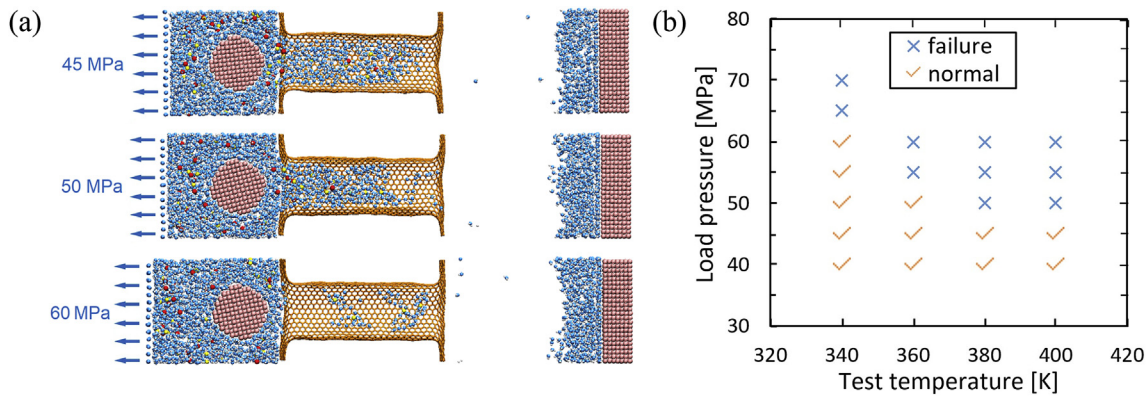

Fig. 2. (a) Sectional views of pumping ability tests after adding load pressure for 1.0 ns with temperatures of 400 K. As the liquid-vapor interface was pinned with load pressure of 45 MPa, and it receded at 50 MPa or 60 MPa, the CNT membrane can provide max pumping pressures of 45–50 MPa at 400 K. (b) Results of pumping ability tests. The regime can provide pumping pressures more than 45 MPa at 340–400 K, and the pumping ability decreases with temperature increasing.

3.3. Mass transfer mechanisms

For the evaporation processes, the driving force of mass transfer should be the vapor pressure difference between two sides. To clarify the mass transfer mechanisms, as shown in Fig. 4-a, the saturation pressures of water and solution, $p_{wat,s}$ and $p_{sol,s}$ were obtained from database of NIST or MD simulations (SI 6) at different equilibrium states [43,44]. It shows that the $p_{wat,s}$ measured by MD, $p_{wat,s,MD}$ were close to the values from NIST, $p_{wat,s,NIST}$, which verified the reliability of the simulation. And the saturation pressure increases quickly with temperature, which can be derived by Clausius–Clapeyron relation. Besides, as the strong interaction from ions reduce the chemical potential of water molecules, the $p_{sol,s}$ measured by MD, $p_{sol,s,MD}$ were a bit smaller than p_{wat} at same equilibrium temperature, and water molecules trend to move from pure to solution in total with $\Delta T = 0$ K shown in Fig. 3-a. Furthermore, it is noted that p_{load} reduced the $p_{sol,s}$ significantly, because external pressure will influence the chemical potential of liquid and change the saturation pressure, which should be the reason why p_{load} reduced the evaporation rates shown in Fig. 3-a. And Fig. 4-b shows the relationship between the distillation rates and Δp_s between solution and fresh sides. The results indicate that the evaporation rates were in direct proportion to Δp_s, and the coefficient was very large, only Δp_s of 0.1 MPa can lead to mass flux of 3.72 ± 0.14 g/(cm^{2}s), which means that the mass transfer ability of the regime is very excellent. The results are good agree with an experiment study in similar condition [45].

3.4. Charge influence

The charge of CNT can intensify the solid-liquid interaction and the pumping ability. As shown in Fig. 5, the system performances with CNT charge of 0e, -3e, -5e, -7e, and −10e were tested at 400 K. The test method of pumping ability is same to that of Fig. 2, and the contact angles were measured on graphene with same charge densities. Results show that with charge increasing, the pumping ability increased and the contact angle decreased due to stronger solid-liquid interaction, which is agree with the electrowetting experiments on graphite [46,47]. But the evaporation rates were not sensitive to CNT charge. Because p_s of liquid depends on its temperature and chemical potential, which approximately equals bulk liquid's, CNT charge has little influence on the mass rate at the same temperature and pressure condition. Besides, as shown in Fig. 5-b, more charge makes it possible to work with higher load pressure, which means that it can output more power with absorbing same heat and get higher energy efficiency, though it will reduce the mass flux.

3.5. Efficiency analysis

As the system has excellent power density, it is necessary to evaluate the power output efficiency. For per mass fresh water gotten, the absolute efficient of power output, η is defined as: $\eta = w_{out}/q_h$, where w_{out} is the output power, q_h is the heat energy absorbed from heat source. Because of fluctuation, getting η accurately by simulation is too costly especially when mass flux is relatively low, but η can be estimated approximately by theory analysis as follows. w_{out} can be estimated by: $w_{out} = p_{load} v_{l,Th}$, where $v_{l,Th}$ is the volume of the evaporated water at T_h. q_h can be estimated by: $q_h = q_c + w_{out}$ for ignoring the system enthalpy change, where q_c is the heat energy absorbed by the cooling wall. Because the heat loss by the conduction and convection can be ignored relative to heat transfer by phase change (SI, Figs. S3–b), q_c can be calculated by: $q_c = h_{v,Th} - h_{l,Tc}$, where $h_{v,Th}$ and $h_{l,Tc}$ are the enthalpy of the vapor and liquid. So η can be estimated by:

$$\eta = \frac{p_{load} v_{l,Th}}{h_{v,Th} - h_{l,Tc} + p_{load} v_{l,Th}} \tag{1}$$

Because each values in equation (1) changed little for the cases

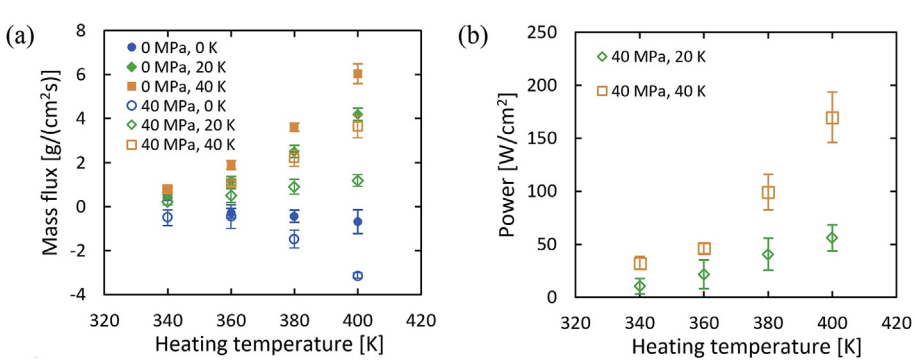

Fig. 3. Rates of self-pumped evaporation: (a) Mass fluxes. The legends show the values of load pressure, p_{load} and the temperature differences, ΔT between the heating rod and cooling wall. The negative mass fluxes at $\Delta T = 0$ K represent water molecules moved from fresh water to solution in total with the driving forces of saturation pressure differences. (b) Power output rates. As the power output relies on the positive movement of piston to overcome the p_{load}, there was no power output when no p_{load} or no positive mass transfer rate at $\Delta T = 0$ K.

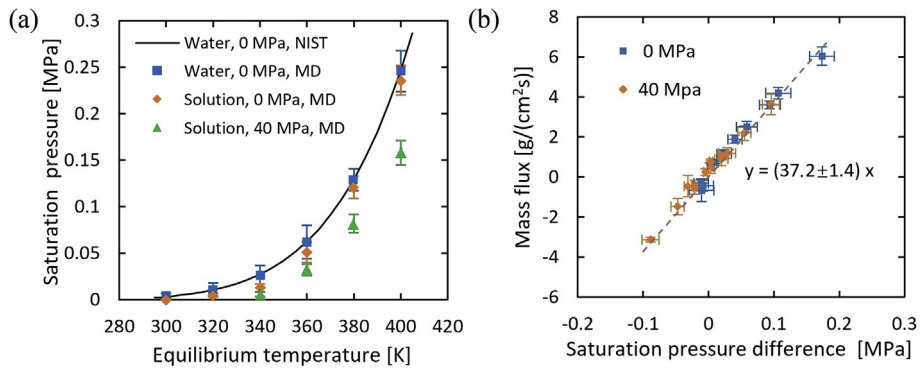

Fig. 4. (a) Saturation pressures of liquids at different equilibrium states. (b) The evaporation rates were in direct proportion to the saturation pressure differences, Δp_s between the solution and the fresh water.

outputted power, the η of the simulations arranged from 1.65% to 1.95%, which changed little, too. But as shown in Fig. 6-a, the relative efficiency η/η_c changed much from 14.1% to 40.4%, where carnot efficiency, η_c is defined as $\eta_c = 1 - T_c/T_h$. It is observed that η/η_c increased with T_h due to larger liquid volume and lower η_c, and η/η_c increased inversely with ΔT for rising of η_c. The η/η_c of the simulations reached maximum of 40.4% when $p_{load} = 40$ MPa, $T_h = 400$ K and $\Delta T = 20$ K. It is reasonable that the system has so large relative efficiency. On the one hand, the heat loss by conduction and convection is relatively little (SI, Figs. S2–b). On the other hand, as shown in Fig. 6-b, because of low thermal resistance of liquid film and little temperature polarization, almost reversible phase changes dominate the processes.

For equation (1), the η and η/η_c depend on p_{load} mainly, so the p_{load} must be large enough to get high efficiency to compete with other power generation methods. However, the efficiency can't increase with p_{load} unlimitedly for two reasons. On the one hand, as shown in Fig. 2, the pumping ability of nano pores restricts the p_{load}. On the other hand, as shown in Fig. 4-a, 4-b p_{load} will reduce p_{sol} and Δp_s and slow down the process. If p_{load} is too large, the Δp_s and the mass flux rate will be negative, and the system will not desalinate water and output power normally.

It is necessary to explore the extreme efficiency of the system. While the thermodynamic property of NaCl solution is too complex to analyze, as shown in Fig. 7, the self-pumped evaporation regime for power output with work media of pure water is analyzed to explore the critical properties of the self-pumping evaporation system. The regime consists of heat sources, work media, a nanoporous membrane, a generator, and flow channels. When the regime is driven by temperature difference of sources, the media will flow circularly with outputting power. As the flow cycle consists of several basic nodes, the efficiency analysis can be based on their thermodynamic and hydromechanical interrelation.

The liquid pressure of inlet is $p_{in,l}$, it decreases to $p_{mem,l}$ under the membrane after flowing across the power generator. The vapor pressures on the membrane and cooling film are $p_{mem,v}$ and $p_{c,v}$, the liquid pressure of cooling film is $p_{c,l}$. The driven force of the cycle is the vapor pressure difference, Δp_v between two sides, equaling $p_{mem,v}$ - $p_{c,v}$. And the driven energy is the temperature difference between two heat sources with temperatures of T_h and T_c. Like equation (1), ignoring the volume work, the system absolute efficiency η can be estimated by:

$$\eta = \frac{p_{out} v_{l,Th}}{h_{v,Th} - h_{l,Tc} + p_{out} v_{l,Th}} \tag{2}$$

where p_{out} is the output pressure.

As liquid pressure will influent the saturation pressure, derived from Gibbs equation [48], the relationship between liquid pressure, p_l and its saturation pressure, $p_{s,pl}$ at a temperature is:

$$\frac{dp_{s,pl}}{dp_l} = \frac{p_{s,pl} v_{l,pl}}{p_s v_v} \tag{3}$$

where $v_{l,pl}$ is the specific volume of liquid with liquid pressure of p_l, and it can be treated as invariant; p_s and v_v are standard saturation pressure and specific vapor volume. So, like Kelvin equation, the saturation pressure in membrane, $p_{mem,s}$ at T_h can be estimated by:

$$p_{mem,s} = p_{s,Th} e^{\frac{(p_{mem,l} - p_{s,Th}) v_{l,Th}}{p_{s,Th} v_{v,Th}}} \tag{4}$$

where $p_{s,Th}$, $v_{l,Th}$, and $v_{v,Th}$ are standard properties of water at T_h.

When the pressure drop between $p_{in,l}$ and $p_{mem,l}$ reaches the limit value, the driving force of mass transfer Δp_v is zero:

$$p_{mem,v} = p_{c,v} \tag{5}$$

The regime is work with no driving force and no mass flux, so vapors are in saturation state equilibrating with liquids. For membrane side:

$$p_{mem,v} = p_{mem,s} \tag{6}$$

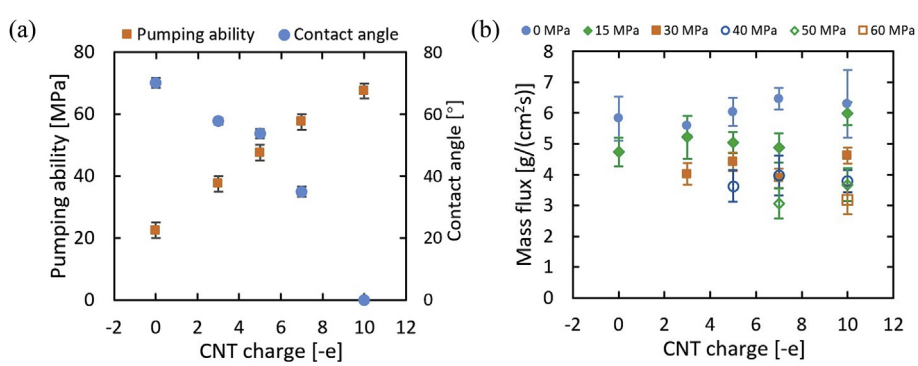

Fig. 5. (a) Pumping abilities and contact angles with different CNT charges at 400 K. (b) The relationship of evaporation rates and CNT charges with $T_h = 400$ K, $\Delta T = 40$ K, and different load pressures.

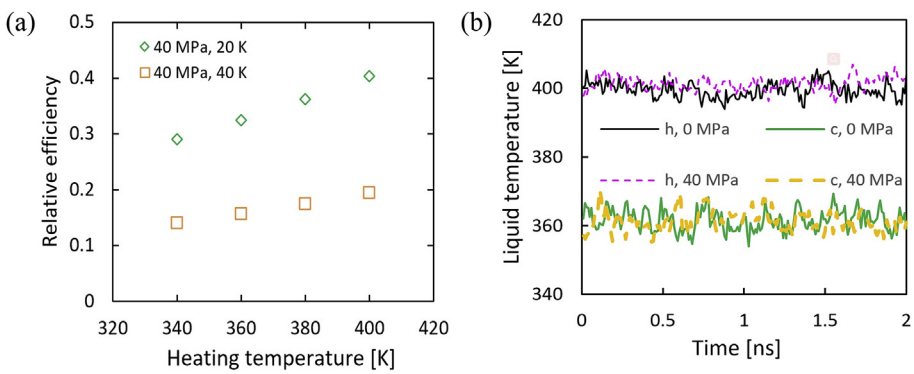

Fig. 6. (a) The relationship between relative efficiency and heating temperature with load pressures of 40 MPa, and temperature differences of 20 or 40 K. (b) Liquid temperatures during the NVE evaporation simulations for two cases with heating temperature of 400 K, cooling temperature of 360 K, and load pressure of 0 MPa or 40 MPa. The liquid temperatures were close to the source temperatures, which means that the thermal resistances between solid wall and liquid-vapor interface are little.

and for cooling side:

$$p_{c,v} = p_{c,l} = p_{s,Tc} \tag{7}$$

where $p_{s,Tc}$ is the standard saturation pressure at T_c.

The pressure drops by flow resistance will be zero too, so:

$$p_{in,l} = p_{c,l} \tag{8}$$

And out pressure is:

$$p_{out} = p_{in,l} - p_{mem,l} \tag{9}$$

From equation (4)–(9), the max output pressure at critical state, $p_{out,cirt}$ can be estimated by:

$$p_{out,crit} = p_{s,Tc} - p_{s,Th} + \frac{p_{s,Th} v_{v,Th}}{v_{l,Th}} (\ln p_{s,Th} - \ln p_{s,Tc}) \tag{10}$$

From equation (2) and (10), the system maximum of absolute efficiency, η_{crit} and critical relative efficiencies, η_{crit}/η_c can be estimated as shown in Fig. 8 with data from NIST [43]. It shows that η_{crit} increases with ΔT for larger vapor difference. η_{crit} is 4.9% with source temperatures of 400 K and 380 K, and it reaches 22.6% with 400 K and 300 K. Because the isothermal phase changes domain the process, the system has outstanding relative efficiency, more than 90% for the analyzed conditions. It is noted that η_{crit}/η_c decreases with ΔT increasing, because of enhancement in irreversible loss, which comes from vapor cooling from T_h to T_c during point 2 to 3 shown in Fig. 7-a.

As shown in Fig. 4-b, a higher Δp_s can get a higher mass flux, which

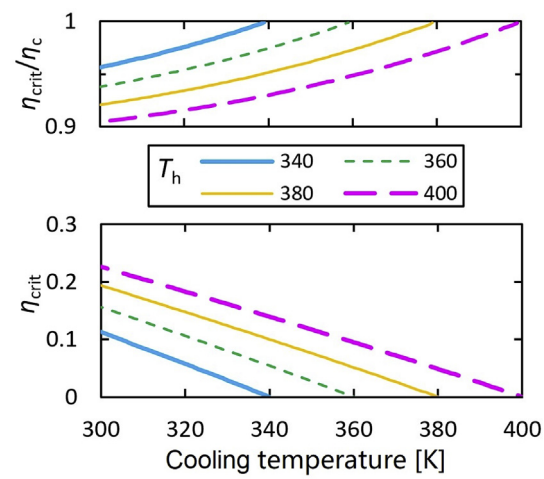

Fig. 8. The critical efficiencies, η_{crit} and critical relative efficiencies, η_{crit}/η_c of self-pumped evaporation system for output power at different heating and cooling temperatures, T_h and T_c.

is important for power density and water desalination. It's obvious that larger ΔT lead to higher Δp_s. Besides, from Fig. 4-a, it is noted that high temperature can get high Δp_s with same ΔT. The relative energy efficiency can be estimated approximately by: $\eta/\eta_c = p_{load} \cdot v_l \cdot T_h / (\Delta h_{lv} \cdot \Delta T)$,

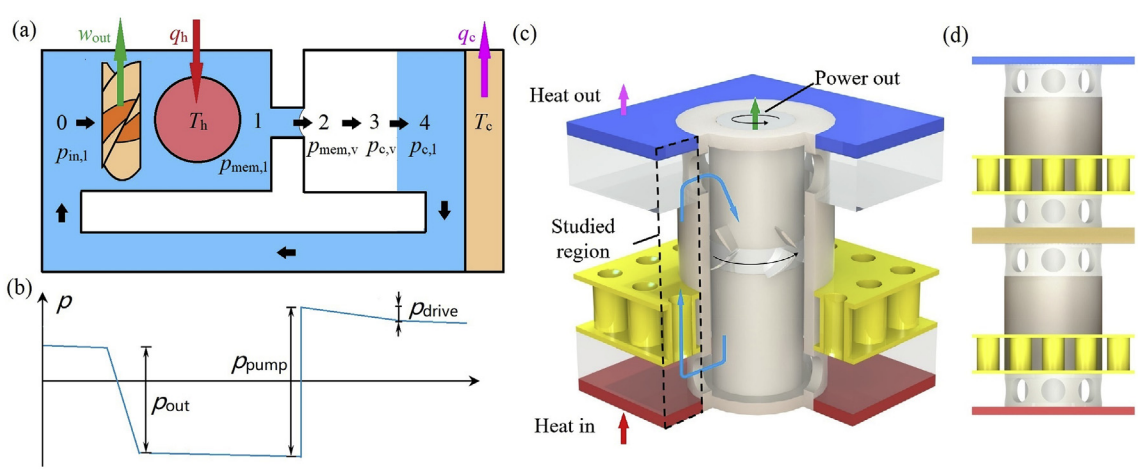

Fig. 7. (a) Schematic of the self-pumped evaporation regime for power output with working medium of pure water. It absorbs and releases heat from two heat sources, and outputs power by the generator in liquid channel. (b) Pressure variation of the process between generator inlet and condensation water outlet. The driving force of the cycle is the vapor difference between point 2 and 3 shown in Fig. 7-a. The vapor difference maintains the evaporation, and generates pumping pressure overcoming the pressure rise in the pore. (c) A configuration for power generation module by self-pump evaporation. The flow cycle is energised by temperature difference between walls, and the power output relies on working liquid flowing across the turbine or other types of generators. (d) The power generation modules can be arranged in series to utilize thermal energy with high temperature difference to avoid too large pumping pressure needed of single stage system.

where $\Delta h_{lv,v}$ is vaporization heat. So, to improve mass flux without affecting the power generation efficiency, it should improve T_h without changing ΔT and p_{load}, or it can improve ΔT and p_{load} simultaneously without changing T_h. And when power generation is less important than water desalination, for example at night, it can reduce p_{load} to get larger mass flux.

4. Discussion

In this study about super high flux self-pumped evaporation, CNTs membrane was chosen as study object for its outstanding properties of flow, heat conduction, and mechanical strength. It can be estimated that the flux is not sensitive to the length of CNT. Because the heat conductivity ability and flow property of CNT is very well, the temperature and vapor pressure of the liquid-vapor interface is not sensitive to the length of CNT, and will not affected the evaporation rates and power generation efficiency significantly. This work can also be extended to other nanoporous membranes for self-pumped evaporation such as AOO membrane, nanoporous silicon membrane, and the membranes with charge added or chemical modification [12,14,49–51]. They have the same basic mechanisms of mass and heat transfer because their structures of nanotubes are similar. However, it should be noted that other type membranes should be treated properly based on their properties. For example, the heat conductive ability of polymer membrane is several orders of magnitude lower than CNTs membrane and it has strong thermal insulation ability, so it is more suitable to apply in solar utilization and vapor generation rather than super high flux evaporation [52].

Although the system has large potential to generate freshwater and power efficiently, it needs more studies to overcome some problems for application. The first is how to supply heat efficiently to achieve the best performance to reduce the investment of membrane. Supplying heat by condensation in heating wall is a feasible method [53], and it can utilize the vapor comes from low-grade heat sources [54]. Another attractive way is utilizing the high-density waste heat from electron devices which generate heat fluxes of 10–1000 W/cm^2 [55]. Because the self-pumped system has low thermal resistance, it can be applied in the thermal management of high power devices like loop heat pipes [56,57].

The second is how to get power efficiently from the capillary flow. Because the liquid pressure under membrane is negative, which is metastable, the flow channel and energy transform machine should be in microscale to avoid vaporization with the help of surface tension. As macro turbine can utilize virtually all pressure drop, nano turbine is an optional device for its best potential performance [58]. Other candidates include fluidic nano generator fiber, streaming potential and so on [59,60].

The third is how to utilize high temperature difference sources efficiently. It must be noted that $p_{out,\ crit}$ computed by equation (10) increases quickly with ΔT, for example, when $T_h = 400$ K, the $p_{out,\ crit}$ is 53 MPa with $\Delta T = 10$ K, but it increased to 109 MPa when $\Delta T = 20$ K, which is difficult to provide by nano-porous membrane even the pore radius is only 1.2 nm. In those simulations, the maximum η_{crit}/η_c of 40.4% was gotten with the case of $T_h = 400$ K and $\Delta T = 20$ K, and for single stage system, η_{crit}/η_c can only be improved to maximum about 50% for the limit of pump pressure less than 50 MPa (Fig. 2). Two ways can break the limit, one is improving the pump capacity by reducing the radius of pores or enhancing the coulomb interaction. Another way is using multistage units in series to reduce ΔT and $p_{out,\ crit}$ of each stage as shown in Fig. 7-d.

5. Conclusions

The ultra-fast self-pumped evaporation for distillation and power output was studied with MD simulations and theory analysis. Because of its high pumping capacity, low heat resistance in liquid, low mass transfer resistance, and low heat loss, self-pumped evaporation has excellent rates and efficiencies with low temperature differences, which brings it large potential for desalination and power generation with consuming low-grade heat.

Declaration of interests

The authors declare no competing financial interest.

Acknowledgments

The study was supported by the National Natural Science Foundation of China (No. 51776079). The authors thank the National Supercomputer Center in Tianjin for providing computing resources.

Appendix A. Supplementary data

Supplementary data to this article can be found online at https://doi.org/10.1016/j.nanoen.2019.104059.

References

[1] A.P. Straub, M. Elimelech, Energy efficiency and performance limiting effects in thermo-osmotic energy conversion from low-grade heat, Environ. Sci. Technol. 51 (2017) 12925–12937, https://doi.org/10.1021/acs.est.7b02213.
[2] N. Ghaffour, T.M. Missimer, G.L. Amy, Technical review and evaluation of the economics of water desalination: current and future challenges for better water supply sustainability, Desalination 309 (2013) 197–207, https://doi.org/10.1016/j.desal.2012.10.015.
[3] D. Cohen-Tanugi, J.C. Grossman, Water desalination across nanoporous graphene, Nano Lett. 12 (2012) 3602–3608, https://doi.org/10.1021/nl3012853.
[4] M. Heiranian, A.B. Farimani, N.R. Aluru, Water desalination with a single-layer MoS2 nanopore, Nat. Commun. 6 (2015) 1–6, https://doi.org/10.1038/ncomms9616.
[5] W. Li, W. Wang, Y. Zhang, Y. Yan, P. Král, J. Zhang, Highly efficient water desalination in carbon nanocones, Carbon N. Y. 129 (2018) 374–379, https://doi.org/10.1016/j.carbon.2017.12.039.
[6] A. Deshmukh, C. Boo, V. Karanikola, S. Lin, A.P. Straub, T. Tong, D.M. Warsinger, M. Elimelech, Membrane distillation at the water-energy nexus: limits, opportunities, and challenges, Energy Environ. Sci. 11 (2018) 1177–1196, https://doi.org/10.1039/c8ee00291f.
[7] K. Zhao, H. Wu, Fast water thermo-pumping flow across nanotube membranes for desalination, Nano Lett. 15 (2015) 3664–3668, https://doi.org/10.1021/nl504236g.
[8] A.A. Hemeda, R.J.A. Esteves, J.T. McLeskey, M. Gad-el-Hak, M. Khraisheh, H. Vahedi Tafreshi, Molecular dynamic simulations of fibrous distillation membranes, Int. Commun. Heat Mass Transf. 98 (2018) 304–309, https://doi.org/10.1016/j.icheatmasstransfer.2018.09.012.
[9] S.C. Maroo, J.N. Chung, Heat transfer characteristics and pressure variation in a nanoscale evaporating meniscus, Int. J. Heat Mass Transf. 53 (2010) 3335–3345, https://doi.org/10.1016/j.ijheatmasstransfer.2010.02.030.
[10] Q. Wang, R. Chen, Ultrahigh flux thin film boiling heat transfer through nanoporous membranes, Nano Lett. 18 (2018) 3096–3103.
[11] T.D. Wheeler, A.S. Stroock, The transpiration of water at negative pressures in a synthetic tree, Nature 455 (2008) 208–212, https://doi.org/10.1038/nature07226.
[12] R. Xiao, S.C. Maroo, E.N. Wang, Negative pressures in nanoporous membranes for thin film evaporation, Appl. Phys. Lett. 102 (2013) 1–5, https://doi.org/10.1063/1.4798243.
[13] Z. Lu, K.L. Wilke, D.J. Preston, I. Kinefuchi, E. Chang-Davidson, E.N. Wang, An ultrathin nanoporous membrane evaporator, Nano Lett. 17 (2017) 6217–6220, https://doi.org/10.1021/acs.nanolett.7b02889.
[14] D.F. Hanks, Z. Lu, J. Sircar, T.R. Salamon, D.S. Antao, K.R. Bagnall, B. Barabadi, E.N. Wang, Nanoporous membrane device for ultra high heat flux thermal management, Microsys. Nanoeng. 4 (2018) 1–10, https://doi.org/10.1038/s41378-018-0004-7.
[15] Y. Li, M.A. Alibakhshi, Y. Zhao, C. Duan, Exploring ultimate water capillary evaporation in nanoscale conduits, Nano Lett. 17 (2017) 4813–4819, https://doi.org/10.1021/acs.nanolett.7b01620.
[16] L. Tocci, T. Pal, I. Pesmazoglou, B. Franchetti, Small scale organic rankine cycle (ORC): a techno-economic review, Energies 10 (2017) 1–26, https://doi.org/10.3390/en10040413.
[17] J. He, T.M. Tritt, Advances in thermoelectric materials research: looking back and moving forward, Science 357 (2017), https://doi.org/10.1126/science.aak9997.
[18] Y. Liu, Y. Chen, J. Ming, L. Chen, C. Shu, T. Qu, Q. Tan, Y. Liu, T. Asefa, Harvesting waste heat energy by promoting H + -ion concentration difference with a fuel cell structure, Nano Energy 57 (2019) 101–107, https://doi.org/10.1016/j.nanoen.2018.12.022.
[19] A.P. Straub, N.Y. Yip, S. Lin, J. Lee, M. Elimelech, Harvesting low-grade heat energy using thermo-osmotic vapour transport through nanoporous membranes, Nat.

Energy. 1 (2016), https://doi.org/10.1038/nenergy.2016.90.
[20] C. Li, K. Liu, H. Liu, B. Yang, X. Hu, Capillary driven electrokinetic generator for environmental energy harvesting, Mater. Res. Bull. 90 (2017) 81–86, https://doi.org/10.1016/j.materresbull.2017.02.022.
[21] M.J. Longhurst, N. Quirke, Temperature-driven pumping of fluid through single-walled carbon nanotubes, Nano Lett. 7 (2007) 3324–3328, https://doi.org/10.1021/nl071537e.
[22] J.K. Holt, H.G. Park, Y. Wang, M. Stadermann, A.B. Artyukhin, C.P. Grigoropoulos, A. Noy, O. Bakajin, Fast mass transport through sub-2-nanometer carbon nanotubes, Science (2006), https://doi.org/10.1126/science.1126298.
[23] E. Pop, D. Mann, Q. Wang, K. Goodson, H. Dai, Thermal conductance of an individual single-wall carbon nanotube above room temperature, Nano Lett. (2006), https://doi.org/10.1021/nl052145f.
[24] E.T. Thostenson, Z. Ren, T.W. Chou, Advances in the science and technology of carbon nanotubes and their composites: a review, Compos. Sci. Technol. (2001), https://doi.org/10.1016/S0266-3538(01)00094-X.
[25] Z. Wang, L. Ci, L. Chen, S. Nayak, P.M. Ajayan, N. Koratkar, Polarity-dependent electrochemically controlled transport of water through carbon nanotube membranes, Nano Lett. 7 (2007) 697–702, https://doi.org/10.1021/nl062853g.
[26] M. Nazari, A. Masoudi, P. Jafari, P. Irajizad, V. Kashyap, H. Ghasemi, Ultrahigh evaporative heat fluxes in nanoconfined geometries, Langmuir (2019), https://doi.org/10.1021/acs.langmuir.8b03463.
[27] X. Dai, F. Yang, R. Yang, Y.C. Lee, C. Li, Micromembrane-enhanced capillary evaporation, Int. J. Heat Mass Transf. (2013), https://doi.org/10.1016/j.ijheatmasstransfer.2013.05.030.
[28] S. Plimpton, Fast parallel algorithms for short-range molecular dynamics, J. Comput. Phys. 117 (1995) 1–42.
[29] W. Humphrey, A. Dalke, K. Schulten, VMD: visual molecular dynamics, J. Mol. Graph. 14 (1996) 33–38, https://doi.org/10.1016/0263-7855(96)00018-5.
[30] C. Vega, J.L.F. Abascal, I. Nezbeda, Vapor-liquid equilibria from the triple point up to the critical point for the new generation of TIP4P-like models: TIP4P/Ew, TIP4P/2005, and TIP4P/ice, J. Chem. Phys. (2006), https://doi.org/10.1063/1.2215612.
[31] V. Prasad K, S.K. Kannam, R. Hartkamp, S.P. Sathian, Water desalination using graphene nanopores: influence of the water models used in simulations, Phys. Chem. Chem. Phys. (2018), https://doi.org/10.1039/c8cp00919h.
[32] E.N. Koukaras, G. Kalosakas, C. Galiotis, K. Papagelis, Phonon properties of graphene derived from molecular dynamics simulations, Sci. Rep. 5 (2015) 1–9, https://doi.org/10.1038/srep12923.
[33] Androulidakis, E.N. Koukaras, J. Parthenios, G. Kalosakas, K. Papagelis, C. Galiotis, Graphene flakes under controlled biaxial deformation, Sci. Rep. 5 (2015) 1–11, https://doi.org/10.1038/srep18219.
[34] A.D. MacKerell, D. Bashford, M. Bellott, R.L. Dunbrack, J.D. Evanseck, M.J. Field, S. Fischer, J. Gao, H. Guo, S. Ha, D. Joseph-McCarthy, L. Kuchnir, K. Kuczera, F.T.K. Lau, C. Mattos, S. Michnick, T. Ngo, D.T. Nguyen, B. Prodhom, W.E. Reiher, B. Roux, M. Schlenkrich, J.C. Smith, R. Stote, J. Straub, M. Watanabe, J. Wiórkiewicz-Kuczera, D. Yin, M. Karplus, All-atom empirical potential for molecular modeling and dynamics studies of proteins †, J. Phys. Chem. B (1998), https://doi.org/10.1021/jp973084f.
[35] D.J. Price, C.L. Brooks, A modified TIP3P water potential for simulation with Ewald summation, J. Chem. Phys. (2004), https://doi.org/10.1063/1.1808117.
[36] H. Los, A. Fasolino, Intrinsic long-range bond-order potential for carbon: performance in Monte Carlo simulations of graphitization, Phys. Rev. B Condens. Matter Mater. Phys. (2003), https://doi.org/10.1103/PhysRevB.68.024107.
[37] W. Li, Y. Yan, M. Wang, P. Král, C. Dai, J. Zhang, Correlated rectification transport in ultranarrow charged nanocones, J. Phys. Chem. Lett. 8 (2017) 435–439, https://doi.org/10.1021/acs.jpclett.6b02640.
[38] S. Nose, A molecular dynamics method for simulations in the canonical ensemble, Mol. Phys. (1984), https://doi.org/10.1080/00268970110089108.
[39] W.G. Hoover, Canonical dynamics: equilibrium phase-space distributions, Phys. Rev. A (1985), https://doi.org/10.1103/PhysRevA.31.1695.
[40] T. Schneider, E. Stoll, Molecular-dynamics study of a three-dimensional one-component model for distortive phase transitions, Phys. Rev. B. (1978), https://doi.org/10.1103/PhysRevB.17.1302.
[41] W. Wang, S. Huang, X. Luo, MD simulation on nano-scale heat transfer mechanism of sub-cooled boiling on nano-structured surface, Int. J. Heat Mass Transf. 100 (2016) 276–286, https://doi.org/10.1016/j.ijheatmasstransfer.2016.04.018.
[42] A. Sam, S.K. Kannam, R. Hartkamp, S.P. Sathian, Water flow in carbon nanotubes: the effect of tube flexibility and thermostat, J. Chem. Phys. (2017), https://doi.org/10.1063/1.4985252.
[43] National Institution of Standards and Technology (NIST), Thermophysical Properties of Fluid Systems. Chemistry Web Book, SDR 69, (2012) https://webbook.nist.gov/chemistry/fluid/ , Accessed date: 10 January 2019.
[44] A.P. Thompson, S.J. Plimpton, W. Mattson, General formulation of pressure and stress tensor for arbitrary many-body interaction potentials under periodic boundary conditions, J. Chem. Phys. (2009), https://doi.org/10.1063/1.3245303.
[45] Z. Lu, I. Kinefuchi, K.L. Wilke, G. Vaartstra, E.N. Wang, A unified relationship for evaporation kinetics at low Mach numbers, Nat. Commun. (2019), https://doi.org/10.1038/s41467-019-10209-w.
[46] D.J. Lomax, P. Kant, A.T. Williams, H.V. Patten, Y. Zou, A. Juel, R.A.W. Dryfe, Ultra-low voltage electrowetting using graphite surfaces, Soft Matter (2016), https://doi.org/10.1039/c6sm01565d.
[47] G. Zhang, M. Walker, P.R. Unwin, Low-Voltage voltammetric electrowetting of graphite surfaces by ion intercalation/deintercalation, Langmuir (2016), https://doi.org/10.1021/acs.langmuir.6b01506.
[48] I.N. Levine, One-component phase equilibrium and surfaces, in: T.L. Hodge (Ed.), Physical Chemistry, sixth ed., McGraw-Hill, New York, 2009, p. 242 https://www.academia.edu/37496770/Physical_Chemistry_6th_ed_-_Levine.pdf.
[49] B. Kakade, R. Mehta, A. Durge, S. Kulkarni, V. Pillai, Electric field induced, superhydrophobic to superhydrophilic switching in multiwalled carbon nanotube papers, Nano Lett. (2008), https://doi.org/10.1021/nl801012r.
[50] Y. Hong, C. Zhu, J. Zhang, J.S. Francisco, X.C. Zeng, Water desalination through rim functionalized carbon nanotubes, J. Mater. Chem. (2018), https://doi.org/10.1039/c8ta10941a.
[51] D. Ostler, S.K. Kannam, P.J. Daivis, F. Frascoli, B.D. Todd, Electropumping of water in functionalized carbon nanotubes using rotating electric fields, J. Phys. Chem. C (2017), https://doi.org/10.1021/acs.jpcc.7b08326.
[52] F. Zhao, X. Zhou, Y. Shi, X. Qian, M. Alexander, X. Zhao, S. Mendez, R. Yang, L. Qu, G. Yu, Highly efficient solar vapour generation via hierarchically nanostructured gels, Nat. Nanotechnol. (2018), https://doi.org/10.1038/s41565-018-0097-z.
[53] S. Gao, W. Liu, Z. Liu, Tuning nanostructured surfaces with hybrid wettability areas to enhance condensation, Nanoscale 11 (2019) 459–466, https://doi.org/10.1039/c8nr05772a.
[54] G. Liu, J. Xu, K. Wang, Solar water evaporation by black photothermal sheets, Nano Energy 41 (2017) 269–284, https://doi.org/10.1016/j.nanoen.2017.09.005.
[55] M. Garven, J.P. Calame, Simulation and optimization of gate temperatures in GaN-on-SiC monolithic microwave integrated circuits, IEEE Trans. Compon. Packag. Technol. 32 (2009) 63–72, https://doi.org/10.1109/TCAPT.2008.2004586.
[56] Y.F. Maydanik, M.A. Chernysheva, V.G. Pastukhov, Review: loop heat pipes with flat evaporators, Appl. Therm. Eng. 67 (2014) 294–307, https://doi.org/10.1016/j.applthermaleng.2014.03.041.
[57] S. He, J. Zhao, Z. Liu, W. Tian, J. Yang, W. Liu, Experimental investigation of loop heat pipe with a large squared evaporator for cooling electronics, Appl. Therm. Eng. 144 (2018) 383–391, https://doi.org/10.1016/J.APPLTHERMALENG.2018.08.075.
[58] J. Li, X. Wang, L. Zhao, X. Gao, Y. Zhao, R. Zhou, Rotation motion of designed nanoturbine, Sci. Rep. 4 (2014) 1–8, https://doi.org/10.1038/srep05846.
[59] Y. Xu, P. Chen, J. Zhang, S. Xie, F. Wan, J. Deng, X. Cheng, Y. Hu, M. Liao, B. Wang, X. Sun, H. Peng, A one-dimensional fluidic nanogenerator with a high power conversion efficiency, Angew. Chem. Int. Ed. 56 (2017) 12940–12945, https://doi.org/10.1002/anie.201706620.
[60] B. Fan, A. Bhattacharya, P.R. Bandaru, Enhanced voltage generation through electrolyte flow on liquid-filled surfaces, Nat. Commun. 9 (2018) 1–7, https://doi.org/10.1038/s41467-018-06297-9.

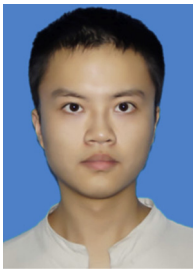

Ji Li received his Bachelor's degree from Huazhong University of Science and Technology (HUST) in 2017 and is now a PhD candidate supervised by Pro. Zhichun Liu in HUST. His research mainly focuses on phase change and heat transfer in nanoscale.

Shan Gao is a doctoral student under the guidance of Pro. Wei Liu in Huazhong University of Science and Technology (HUST), he received his B.S degree from HUST in 2015. His scientific interest main focuses on droplets bounce and condensation in nanoscale.

Rui Long is lecture of the School of Energy and Power Engineering, Huazhong University of Science and Technology (HUST). He received his Bachelor degree (2011) and Doctoral degree (2016) in HUST. He mainly engaged in non-equilibrium thermodynamics theory, renewable energy, low-grade heat harvesting, nanoscale anti-electrodialysis and ion transport characteristics. As the first author or correspondent author, he published 28 academic papers included in SCI.

Wei Liu is professor of the School of Energy and Power Engineering, Huazhong University of Science and Technology. He has been engaged in teaching and research of heat transfer, energy conservation, electronic cooling, and porous media. He published two textbooks, three academic monographs, and 220 academic papers included in SCI. His H factor is 50. He also authorized 16 national invention patents. He enjoys the government subsidy of the State Council. He is member of the China Society of Engineering Thermophysics, and former director of China Renewable Energy Society.

Zhichun Liu is professor in the School of Energy and Power Engineering, Huazhong University of Science and Technology of China (HUST). He received his Ph.D. from HUST in 2006, and was visiting scholar in Massachusetts Institute of Technology, US in 2012. His research focuses on heat transfer in nanoscale, electronic cooling, porous media and energy conservation. He published 66 academic papers included in SCI.